Chirality-Induced Asymmetric Magnetic Nucleation in $Pt/Co/AlO_x$ Ultrathin Microstructures

S. Pizzini,[1,2,*] J. Vogel,[1,2] S. Rohart,[3] L. D. Buda-Prejbeanu,[4] E. Jué,[4] O. Boulle,[4] I. M. Miron,[4]
C. K. Safeer,[4] S. Auffret,[4] G. Gaudin,[4] and A. Thiaville[3]

[1]*CNRS, Institut Néel, 38042 Grenoble, France*
[2]*Univ. Grenoble Alpes, Institut Néel, 38042 Grenoble, France*
[3]*Laboratoire de Physique des Solides, Univ. Paris-Sud, CNRS UMR 8502, 91405 Orsay, France*
[4]*SPINTEC, UMR 8191, CEA/CNRS/UJF/Grenoble-INP, INAC, 38054 Grenoble Cedex, France*
(Received 16 March 2014; published 23 July 2014)

The nucleation of reversed magnetic domains in $Pt/Co/AlO_x$ microstructures with perpendicular anisotropy was studied experimentally in the presence of an in-plane magnetic field. For large enough in-plane field, nucleation was observed preferentially at an edge of the sample normal to this field. The position at which nucleation takes place was observed to depend in a chiral way on the initial magnetization and applied field directions. A quantitative explanation of these results is proposed, based on the existence of a sizable Dzyaloshinskii-Moriya interaction in this sample. Another consequence of this interaction is that the energy of domain walls can become negative for in-plane fields smaller than the effective anisotropy field.

Chirality is a fascinating property of nature [1]. It was discovered in 1848 by Pasteur, by correlating the optical activity of molecules in solution to the hemihedral shape of the crystals that they form [2]. More generally, chiral textures often appear in physics as a result of symmetry breaking, either spontaneously, for example, in macroscopic quantum systems [3], or when stabilized by a chiral interaction as in liquid crystals [4] or magnetism [5]. In the latter case, the transcription of the chirality from the atomic scale to the macroscopic scale of textures may be impeded by the existence of an anisotropy. This is exemplified in liquid crystals, where under a dc magnetic or electric field that induces anisotropy, the cholesteric-nematic transition takes place [4]. Thus, the detection and quantification of a chiral interaction when it is too weak to give rise to a global chiral texture is difficult.

Magnetism is another prominent field where chiral textures are considered. A chiral magnetic interaction indeed exists, namely, an antisymmetric exchange called the Dzyaloshinskii-Moriya interaction (DMI) [5,6], that is allowed when central symmetry is broken. In many compounds having this property, especially the cubic B20 structures with depressed magnetic anisotropy, chiral textures like homochiral spin spirals or 2D Skyrmion lattices have been observed, both in reciprocal [7] and in real space [8]. Another class of chiral magnetic systems has recently appeared, namely, the few atomic layer thick samples grown on an underlayer with large spin-orbit interaction, showing structural inversion asymmetry and perpendicular magnetic anisotropy (PMA) [9–12]. In these systems, PMA may be very strong so that chiral spin spirals are not stable, and as a result, for ultrathin films in ambient conditions, the DMI has

remained unnoticed for about 20 years. However, at magnetic edges like a domain wall (DW) separating two uniformly magnetized domains or at physical edges in a microstructure, the competition of chiral interaction with anisotropy is modified. Indeed, the peculiarities of field and current-induced dynamics of domain walls in such samples [13–15] have been found to be consistent with a chiral texture localized on the DW, deriving from the presence of the interface-induced DMI [16]. These local chiral magnetization textures, which appear as Néel walls of a fixed chirality, have also been observed recently by low-energy electron microscopy [17,18], on samples with wide domain walls.

In this Letter we show that chiral interactions can also be detected at the edges of a microstructure: in the presence of an additional in-plane field, nucleation of reversed domains takes place preferentially at one edge of the sample, oriented perpendicular to this field. The side at which nucleation takes place depends on the direction of both the additional field and the initial magnetization. This asymmetry is thus chiral, and we show that the DMI can explain this chirality as well as the values of the nucleation field.

The experiments were carried out on $Pt(3 \text{ nm})/Co(0.6 \text{ nm})/AlO_x(2 \text{ nm})$ layers patterned by electron beam lithography into two large injection pads connected by micrometric strips. The strips were used for field and current-driven domain wall dynamics (not shown here) while the nucleation experiments were carried out on the pads. The films were deposited on a Si/SiO_2 substrate by magnetron sputtering. Samples were oxidized *in situ* by oxygen plasma in order to induce PMA [19]. Magnetization reversal was studied using magneto-optical Kerr microscopy. In each experiment, magnetization was
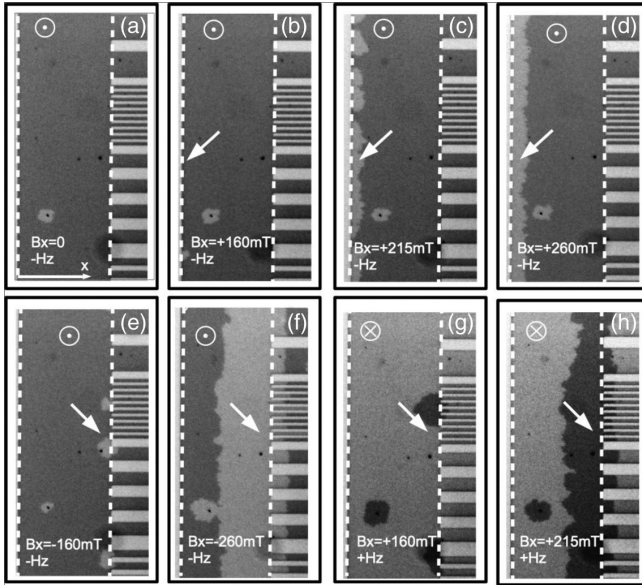
FIG. 1.   Kerr images showing the chiral nucleation of domains at one edge of the pad of the $Pt/Co/AlO_x$ microstructure, by application of an out-of-plane field pulse. (a)–(d) Magnetization is initially saturated $\uparrow$ and $B_x = 0$, +160, +215, and +260 mT, (e)—(f) magnetization is initially saturated $\uparrow$ and $B_x = -160$ and -260 mT, (g)–(h) magnetization is initially saturated $\downarrow$ and B_x is +160 and +260 mT. The width of the pad is 70 μm. The dotted lines highlight the left and right edges of the pad and the arrows show the side of the sample where nucleation takes place.

first saturated with an out-of-plane magnetic field (H_z). Nucleation of reversed domains was then induced by an opposite H_z field pulse, under a dc in-plane field H_x. Several samples with similar composition and varying magnetic anisotropy were measured.

Figure 1 illustrates an example of the occurrence of chiral nucleation and the symmetry of this effect. When an H_z field pulse (amplitude 18–20 mT and length 50–100 ms) is applied antiparallel to the initial magnetization direction, magnetization reversal is initiated by the nucleation of a reversed domain at a particular spot of the sample, away from the edges, corresponding to a local defect [Fig. 1(a)]. When a sufficiently strong in-plane field H_x is applied at the same time as H_z, new nucleation centers appear at one edge of the pad. Starting from positive ($\uparrow$) saturation (corresponding to dark contrast in the Kerr images), a positive H_x field (along the positive x axis) promotes nucleation of reversed $\downarrow$ domains at the left edge of the sample [Figs. 1(b)–1(d)]. As the amplitude of H_x increases, the nucleation probability increases but no nucleation appears at the right edge of the sample, up to $\mu_0 H_x = 260$ mT. If either the initial magnetization direction or the H_x field direction is reversed, the nucleation takes place at the opposite edge. Figures 1(e)–1(f) show indeed that nucleation takes place at the right edge when a negative H_x field is applied starting from the same $\uparrow$ saturation. Similarly, nucleation takes place on the right edge when H_x
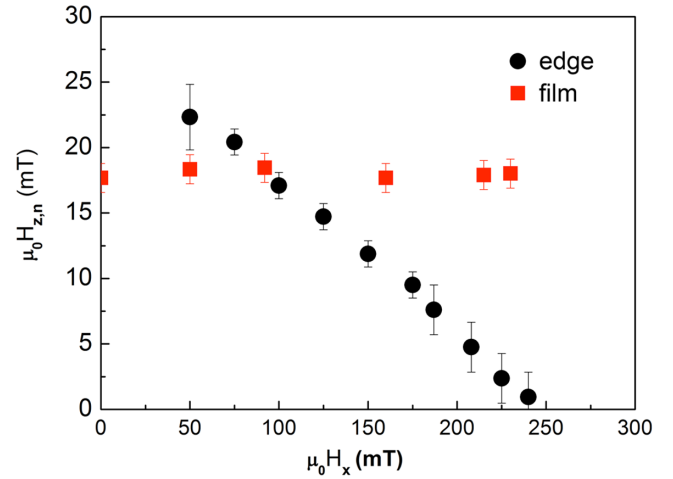
FIG. 2 (color online).   Nucleation fields measured as a function of in-plane field H_x for the reversed domain in the middle (squares) and at the left edge of the sample (circles). Note the difference of scales between the two axes.

is kept positive but the initial magnetization is reversed ($\downarrow$) [Figs. 1(g)–1(h)]. This shows that the observed asymmetry is indeed chiral.

The nucleation field $H_{z,n}$ was measured as a function of H_x for a sample having an anisotropy field of 700 mT (slightly weaker than that of the sample shown in Fig. 1) both for a defect within the film and at the sample edges. The length of the H_z pulse was fixed at 20 ms. For a defect within the film, $H_{z,n}$ was defined as the field for which the domain appears with 100% probability. For the edges, $H_{z,n}$ was defined as the field for which 10–15 domains systematically nucleate [20]. The main result of these measurements, shown in Fig. 2, is that while the nucleation field of a domain within the film is almost H_x-field independent, $H_{z,n}$ strongly decreases with the in-plane field for the domains nucleating at the sample edges.

The chiral behavior of magnetization reversal cannot be explained by simply invoking a local reduction of anisotropy along the sample edges, which would keep the symmetry between opposite edges. In order to explain the observed chiral nucleation, a phenomenon which breaks the symmetry of the system when an H_x field is applied has to be invoked. A possible origin of this phenomenon is the presence in noncentrosymmetric $Pt/Co/AlO_x$ stacks of a nonvanishing DM interaction, which has already been invoked to explain the stabilization of chiral Néel walls, called Dzyaloshinskii domain walls (DDW) [16]. We thus quantitatively investigate this hypothesis using two models.

Zero temperature model.—In real samples (i.e., including defects), magnetization reversal is controlled by few defects acting as nucleation centers [27]. Chiral nucleation requires defects with a chiral micromagnetic structure around them. The DMI provides such a state at sample edges, inducing locally a tilt of the magnetization [28]. When an in-plane field normal to an edge is applied, the tilt angle depends on
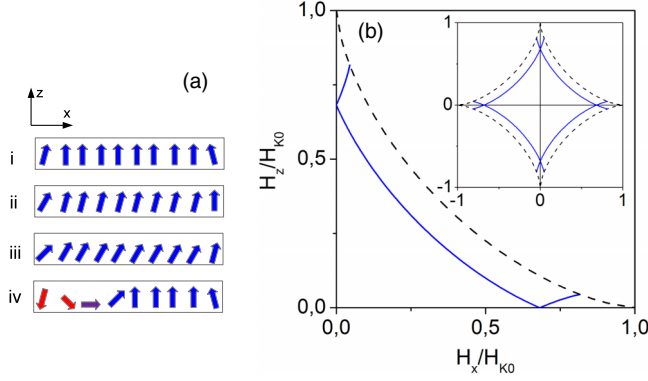
FIG. 3 (color online). (a) Sketch of the micromagnetic configuration within a microstructure with the DMI in zero applied field (i), under an x field (ii), under an additional negative z field (iii), and after reversal, with a domain wall of magnetization parallel to the x field (iv). (b) results of a 1D calculation showing the reversal field for $D/D_{c0} = 0$ (dashes) and 0.5 (lines). For $D \neq 0$ an easy and a hard branch develop, corresponding to the reversal at the two edges of the microstructure. Inset: complete astroids.

its orientation (parallel or antiparallel to the field) and preferential nucleation at one edge can be expected. Using the same 1D model in the x direction normal to the edge as in [28], the edge tilt angle θ is given by

$$m_x = \sin \theta = \pm\Delta \frac{D}{2A} + \frac{H_x}{H_{K_0}}, \tag{1}$$

where D is the DMI constant, A the exchange constant, $H_{K_0} = 2K_0/(\mu_0 M_s)$ the anisotropy field (K_0 is the effective anisotropy constant), $\Delta = \sqrt{A/K_0}$ the nominal domain wall width, and the $\pm$ sign refers to the two edges of the sample along x. Figure 3(a) sketches the effect of H_x and H_z on the micromagnetic configurations.

In the absence of thermal fluctuations, the solution for the onset of magnetization instability at the edge can be mapped [20] to a solution of the Stoner-Wohlfarth model [29]. Figure 3(b) shows the reversal field H_z vs H_x (normalized to H_{K_0}), calculated for different D/D_{c0} values (with $D_{c0} = 4\sqrt{AK_0}/\pi \equiv \sigma_{00}/\pi$ giving the onset of the spontaneous formation of magnetization cycloids). For $D = 0$, the standard Stoner-Wohlfarth astroid is obtained and no difference occurs between the sample edge and the center. For a finite D, the edge reversal field with $H_x = 0$ decreases by a factor $[1 - (2/\pi)D/D_{c0}]$. As H_x is applied, the astroid splits into two branches revealing the difference between the two sample sides: on the side where m_x is initially parallel (antiparallel) to H_x the tilt is larger (smaller) and the reversal field decreases (increases) with H_x.

This model is in qualitative agreement with the experimental results: (i) it explains why in the presence of the DMI magnetic nucleation is observed only at one sample edge, (ii) it explains qualitatively the decrease of the nucleation

field as the H_x field amplitude is increased. However, the calculated values of the nucleation field are about 1 order of magnitude larger than the experimental ones.

Finite temperature model.—In a macroscopic sample, magnetization reversal occurs *via* the creation of reversed domains followed by the propagation of domain walls. This is described by the so-called "droplet model" [30,31], well known for first order phase transitions. Let us first consider the creation of a cylindrical domain of radius R inside the film. The free energy of this droplet is

$$E/t = 2\pi R\sigma_0 - 2\mu_0 M_s H_z \pi R^2, \tag{2}$$

where t is the film thickness, $\sigma_0 = \sigma_{00}(1 - D/D_{c0})$ the domain wall energy density in the presence of the DMI [16], and H_z the applied magnetic field. The critical droplet radius is $R_c = \sigma_0/(2\mu_0 M_s H_z)$. Below R_c the droplet collapses, whereas above R_c the domain increases its size by DW propagation. This gives rise to an energy barrier for the nucleation of the droplet:

$$E_B = \frac{\pi \sigma_0^2 t}{2\mu_0 M_s H_z}. \tag{3}$$

In an Arrhenius model with attempt time τ_0, the nucleation field for a waiting time $\tau = \tau_0 e^p$ reads then

$$H_{n,film} = \frac{\pi \sigma_0^2 t}{2\mu_0 M_s p k_B T}. \tag{4}$$

Under the assumption that the magnetic droplet structure is completely rigid (i.e., no magnetization rotation in the domains nor in the domain wall, no droplet shape optimization), the application of an in-plane field H_x does not modify the energy of the droplet: the Zeeman energy gained within the half droplet having a DW magnetization component parallel to H_x is compensated by the loss of energy within the half droplet with opposite magnetization. This agrees with the results of Fig. 2, which show that the nucleation field for the reversed domain away from the edges does not vary with H_x.

On the other hand, the energy of a half-droplet nucleating at one edge of the sample is modified by the in-plane field. By again assuming a rigid droplet structure, its energy reads

$$E/t = \pi R(\sigma_0 \mp 2\Delta\mu_0 M_s H_x) - \mu_0 M_s H_z \pi R^2, \tag{5}$$

where the Zeeman energy associated with the in-plane field H_x within the DW volume has been included in the DW energy. The $\mp$ sign refers to the gain or loss of Zeeman energy for a domain wall having its magnetization parallel or antiparallel to the applied in-plane field, respectively, i.e., to the two sample edges. In analogy with the nucleation within the film, the nucleation field at the edges is then
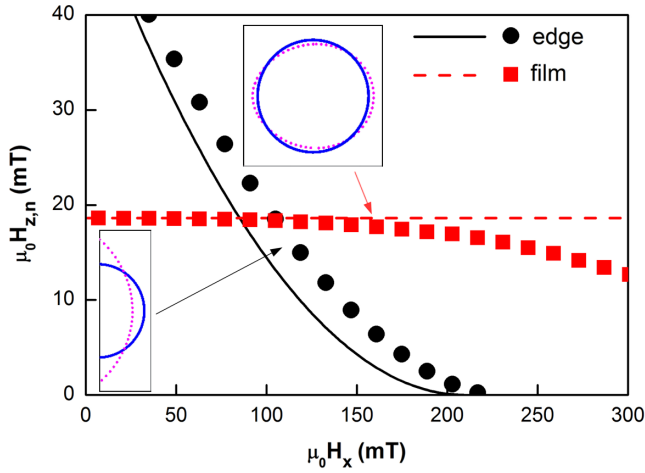
FIG. 4 (color online). Nucleation field vs H_x for a domain at the edge and in the film calculated using the rigid droplet model (full and dotted line) and the relaxed model (dots and square symbols). Insets: calculated droplet shapes for $H_x/H_{K_0} = 0$ (lines) and 0.21 (dots).

$$H_{n,edge} = \frac{\pi(\sigma_0 \mp 2\Delta\mu_0 M_s H_x)^2 t}{4\mu_0 M_s p k_B T}. \qquad (6)$$

This shows that the presence of the DMI gives rise to different nucleation fields for DW having magnetization parallel or antiparallel to H_x. In a sample with the DMI, the DDW created at the two edges starting from saturation have opposite magnetization: this explains the nucleation of reversed domains only at one side of the sample and the symmetry of the effect when the in-plane field direction and magnetization saturation are reversed. Note that, experimentally, nucleation at the hard side of the sample is never observed at larger H_z fields, as the magnetization is always reversed by propagation of the domain walls formed at the easy side for smaller nucleation fields.

Figure 4 (lines) shows the variation of the nucleation field as a function of H_x, calculated for a droplet within the film and a half-droplet having its magnetization parallel to the applied field. The used magnetic parameters for Pt/Co/AlO$_x$ are $A = 16$ pJ/m, $M_s = 1.1$ MA/m, $\mu_0 H_{K_0} = 700$ mT, and $D = 2.2$ mJ/m^2 ($D/D_{c0} = 0.7$).

It can be seen that the droplet model including the presence of large the DMI provides an excellent understanding of the measurements: not only the different variation of $H_{z,n}$ vs H_x within the film and at the easy edge is accounted for, but also the order of magnitude of the reversal fields at the edge is in quantitative agreement with the experiments. In the film, in order to account for the local reduction of the anisotropy field at the defect and, therefore, reproduce the experimental values of the nucleation field, the energy of the domain wall was reduced by a factor $\epsilon \approx 0.4$ as done previously [32]. Note that the difference between the theoretical and the experimental curve while approaching the x axis can be explained by the nonperfect

compensation of the tilt of the H_x field with respect to the sample surface.

Lifting the first two restrictions of the rigid model can be performed semianalytically, using the "small circle" model (the wall magnetization distribution is assumed to belong to a plane, that cuts the order parameter sphere along a small circle). This provides accurate DW energies, as was shown long ago [33] and checked again here. Once the orientation-dependent DW energy is known, the optimal droplet shape is obtained using the Wulff construction [34]. In the case of the half droplet, in full analogy with the calculation of the contact angle of a liquid droplet on a surface, the difference of edge energies for up and down domain magnetization (that can be analytically calculated with the same model as used in the Zero temperature section) was introduced in the Wulff construction. For each value of H_x, the droplet shapes were first computed (see insets in Fig. 4). Inside the film, an asymmetric elongation along the in-plane field is seen. At the edge, a significant elongation perpendicular to the field takes place, as the DW oriented perpendicular to the field has a much reduced energy and can expand its length. With the shape fixed, the determination of the critical droplet size was then performed [20]. The numerical results of this semianalytical model, shown in Fig. 4 (symbols) for the case $D/D_{c0} = 0.7$, are very close to experiments. The new feature is the decrease of the nucleation field at the defect in the film, as the in-plane field increases. Comparing calculations and experimental data showed that, within this model, $D \geq 0.7D_{c0}$ is required to get similar evolutions with in-plane field magnitude [20].

The decrease to zero of the nucleation field, seen both experimentally and in the model, is due to the decrease to zero of the DDW energy under a sufficiently large in-plane field. In the case of an in-plane field normal to the DDW, the DW profile can be analytically calculated for an arbitrary value of the in-plane field. For DMI-induced DW moment in the same direction as the field, the DW energy reads (with $h = H_x/H_{K_0}$ [35]):

$$\sigma = \sigma_{00}\left[\sqrt{1-h^2} - \left(h + \frac{2}{\pi}\frac{D}{D_{c0}}\right)\arccos h\right]. \qquad (7)$$

This falls to zero at $h \approx 1 - D/D_{c0}$. For other in-plane angles between field and DW normal, the zero crossing takes place at larger fields, reaching H_{K_0} when the field is along the DW. This appears to be a unique feature of the Dzyaloshinskii DW.

In conclusion, the nucleation of reversed domains in Pt/Co/AlO$_x$ microstructures was observed to be chiral, and could be explained by the presence of a strong DM interaction, already identified as being responsible for the chiral texture of domain walls, observed in some noncentrosymmetric systems. Asymmetric nucleation measurements constitute a straightforward way to determine the

sign of D and therefore the chirality of Néel walls. Note that edge nucleation of reversed domains bypasses the topological problem of nucleating skyrmions inside a sample [36,37].

A droplet model including DMI gives quantitative agreement with the measurements, even when assuming a complete rigidity of the magnetic structures. A full treatment of the domain wall profile shows that for large DMI and in-plane field much lower than the anisotropy field the DDW energy becomes negative, a feature hitherto unnoticed. Although all consequences of this specific feature of the Dzyaloshinskii domain walls need to be explored, we already observed nucleation of reversed domains under the application of the sole H_x field.

---

* stefania.pizzini@neel.cnrs.fr

[1] K. Mislow, *Molecular Chirality*, Topics in Stereochemistry Vol. 22, edited by S. E. Denmark (Wiley, New York, 1999), p. 1.

[2] The word chirality was introduced later by Lord Kelvin, in 1893 [1].

[3] G. E. Volovik and M. Krusius, Physics **5**, 130 (2012).

[4] P.-G. de Gennes and J. Prost, *The Physics of Liquid Crystals,* 2nd. ed. (Oxford University Press, New York, 1993).

[5] I. E. Dzyaloshinskii, Sov. Phys. JETP **5**, 1259 (1957).

[6] T. Moriya, Phys. Rev. **120**, 91 (1960).

[7] S. Mühlbauer, B. Binz, F. Jonietz, C. Pfleiderer, A. Rosch, A. Neubauer, R. Georgii, and P. Böni, Science **323**, 915 (2009).

[8] X. Z. Yu, Y. Onose, J. H. Park, J. H. Han, Y. Matsui, N. Nagaosa, and Y. Tokura, Nature (London) **465**, 901 (2010).

[9] M. Bode, M. Heide, K. von Bergmann, P. Ferriani, S. Heinze, G. Bihlmayer, A. Kubetzka, O. Pietzsch, S. Blügel, and R. Wiesendanger, Nature (London) **447**, 190 (2007).

[10] S. Meckler, N. Mikuszeit, A. Pressler, E. Y. Vedmedenko, O. Pietzsch, and R. Wiesendanger, Phys. Rev. Lett. **103**, 157201 (2009).

[11] I. M. Miron, G. Gaudin, S. Auffret, B. Rodmacq, A. Schuhl, S. Pizzini, J. Vogel, and P. Gambardella, Nat. Mater. **9**, 230 (2010).

[12] I. M. Miron, T. Moore, H. Szambolics, L. D. Buda-Prejbeanu, S. Auffret, B. Rodmacq, S. Pizzini, J. Vogel, M. Bonfim, A. Schuhl, and G. Gaudin, Nat. Mater. **10**, 419 (2011).

[13] S. Emori, U. Bauer, S.-M. Ahn, E. Martinez, and G. S. D. Beach, Nat. Mater. **12**, 611 (2013).

[14] K.-S. Ryu, L. Thomas, S.-H. Yang, and S. Parkin, Nat. Nanotechnol. **8**, 527 (2013).

[15] S.-G. Je, D.-H. Kim, S.-C. Yoo, B.-C. Min, K.-J. Lee, and S.-B. Choe, Phys. Rev. B **88**, 214401 (2013).

[16] A. Thiaville, S. Rohart, E. Jué, V. Cros, and A. Fert, Europhys. Lett. **100**, 57002 (2012).

[17] G. Chen, T. Ma, A. T. N'Diaye, H. Kwon, C. Won, Y. Wu, and A. K. Schmid, Nat. Commun. **4**, 2671 (2013).

[18] G. Chen, J. Zhu, A. Quesada, J. Li, A. T. N'Diaye, Y. Huo, T. P. Ma, Y. Chen, H. Y. Kwon, C. Won, Z. Q. Qiu, A. K. Schmid, and Y. Z. Wu, Phys. Rev. Lett. **110**, 177204 (2013).

[19] A. Manchon, S. Pizzini, V. Uhlíř, J. Vogel, L. Lombard, C. Ducruet, S. Auffret, B. Rodmacq, B. Dieny, M. Hochstrasser, and G. Panaccione, J. Magn. Magn. Mater. **320**, 1889 (2008).

[20] See Supplemental Material at http://link.aps.org/supplemental/10.1103/PhysRevLett.113.047203, which gives more information about the experimental technique and procedure, details the solution of the zero temperature model, shows full numerical micromagnetic simulation results, explains how the micromagnetic parameters of the sample were estimated, and includes Refs. [21–26].

[21] A. Thiaville, J. Magn. Magn. Mater. **182**, 5 (1998).

[22] M. Jamet, W. Wernsdorfer, C. Thirion, D. Mailly, V. Dupuis, P. Mélinon, and A. Pérez, Phys. Rev. Lett. **86**, 4676 (2001).

[23] C. Vouille, A. Thiaville, and J. Miltat, J. Magn. Magn. Mater. **272**, E1237 (2004).

[24] L. D. Buda, I. L. Prejbeanu, U. Ebels, and K. Ounadjela, Comput. Mater. Sci. **24**, 181 (2002).

[25] O. Boulle, S. Rohart, L. D. Buda-Prejbeanu, E. Jué, I. M. Miron, S. Pizzini, J. Vogel, G. Gaudin, and A. Thiaville, Phys. Rev. Lett. **111**, 217203 (2013).

[26] P. J. Metaxas, J. P. Jamet, A. Mougin, M. Cormier, J. Ferré, V. Baltz, B. Rodmacq, B. Dieny, and R. L. Stamps, Phys. Rev. Lett. **99**, 217208 (2007).

[27] A. Aharoni, Rev. Mod. Phys. **34**, 227 (1962).

[28] S. Rohart and A. Thiaville, Phys. Rev. B **88**, 184422 (2013).

[29] E. C. Stoner and E. P. Wohlfarth, Phil. Trans. R. Soc. A **240**, 599 (1948); reprinted in IEEE Trans. Magn. **27**, 3475 (1991).

[30] B. Barbara and M. Uehara, IEEE Trans. Magn. **12**, 997 (1976).

[31] B. Barbara, J. Magn. Magn. Mater. **129**, 79 (1994).

[32] J. Moritz, B. Dieny, J.-P. Nozières, Y. Pennec, J. Camarero, and S. Pizzini, Phys. Rev. B **71**, 100402 (2005).

[33] A. Hubert, *Theorie der Domänenwände in geordneten Medien* (in german) (Springer Verlag, Berlin, 1974).

[34] M. C. Desjonquères and D. Spanjaard, *Concepts in Surface Physics*, Springer Series in Surface Sciences Vol. 30 (Springer, Berlin, 1996).

[35] The calculation without the DMI can be found in [33].

[36] J. Sampaio, V. Cros, S. Rohart, A. Thiaville, and A. Fert, Nat. Nanotechnol. **8**, 839 (2013).

[37] O. J. Lee, L. Q. Liu, C. F. Pai, Y. Li, H. W. Tseng, P. G. Gowtham, J. P. Park, D. C. Ralph, and R. A. Buhrman, Phys. Rev. B **89**, 024418 (2014).